JAAS

Accepted Manuscript

This is an *Accepted Manuscript*, which has been through the Royal Society of Chemistry peer review process and has been accepted for publication.

Accepted Manuscripts are published online shortly after acceptance, before technical editing, formatting and proof reading. Using this free service, authors can make their results available to the community, in citable form, before we publish the edited article. We will replace this *Accepted Manuscript* with the edited and formatted *Advance Article* as soon as it is available.

You can find more information about *Accepted Manuscripts* in the Information for Authors.

Please note that technical editing may introduce minor changes to the text and/or graphics, which may alter content. The journal's standard Terms & Conditions and the Ethical guidelines still apply. In no event shall the Royal Society of Chemistry be held responsible for any errors or omissions in this *Accepted Manuscript* or any consequences arising from the use of any information it contains.

ROYAL SOCIETY OF CHEMISTRY

www.rsc.org/jaas

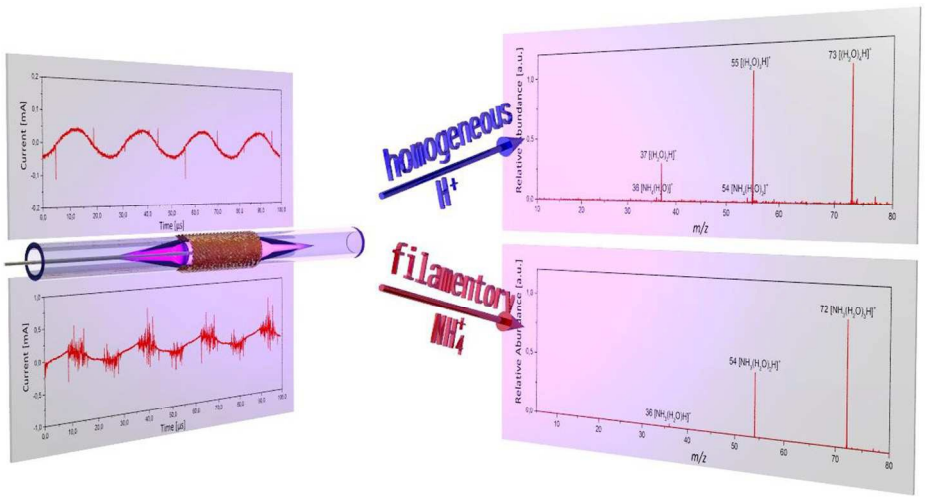

447x225mm (72 x 72 DPI)

Characterization of two modes in a dielectric barrier discharge probe by optical emission spectroscopy and time-of-flight mass spectrometry

Andreas Bierstedt[a], Ulrich Panne[a,b], Knut Rurack[a], Jens Riedel[a]

a BAM, Federal Institute for Materials Research and Testing, Richard-Willstätter-Straße 11, 12489 Berlin, Germany

b Humboldt-University Berlin, Department of Chemistry, Brook-Taylor-Straße 2, 12489 Berlin, Germany

Corresponding author: Jens Riedel, Email: Jens.Riedel@bam.de, Phone: +49 30 8104-1162, Fax: +49 30 8104-1167

Keywords: Dual mode, Dielectric barrier discharge, Ambient desorption/ionization mass spectrometry, Emission spectroscopy, Ionization

ABSTRACT (50-250 words)

Among the large number of new ambient ionization schemes in the last years, the dielectric barrier discharge (DBD) witnessed special attention. In this contribution a versatile dual mode DBD is introduced and characterized by means of optical emission spectroscopy and time-of-flight mass spectrometry. A direct comparison of the individual results from spectroscopy, spectrometry and transient current/voltage consumption gives evidence for the existence of two individual operational mechanisms. The first is driven by rapid transient changes in the potential difference between the two electrodes over time (usually denoted homogeneous mode), while the second is caused at high static potential differences (leading to filamentary discharges). The transient versus steady-state character of the individual discharge origin suggest the driving force for the current flow to be inductive and capacitive, respectively. In most cases of dielectric barrier plasmas both discharge types coexist as competitive ion formation channels, however, detailed plasma characteristics of DBDs operated under different conditions allow for a clear distinction of the individual contributions. In this way, two characteristic product channels for the ionization of ambient water could be observed resulting in the generation of either preferentially protonated water clusters or ammonium water clusters. Careful tuning of the operation parameters of the discharge device allows an operation predominated by either of the two modes. As a consequence, facile switching into the desired operational mode yields in either protonated molecules or ammoniated molecules of the analyte. Plasma characteristics for both moieties were evaluated and cross-correlated on the basis of several factors including: the production of reagent ions, the individual appearance of current/voltage profiles, UV/Vis spectroscopy, voltage and flux dependence and the individual response to test compounds. Whereas the filamentary mode has been already discussed in literature to induce fragmentation processes, no experimental evidence for analyte dissociation could be examined in the case of the used test compounds.

Introduction

In recent years, various atmospheric plasma techniques have been introduced as ionization sources for ambient mass spectrometry (MS) applications.[1–3] Among these are Direct Analysis in Real-time (DART)[4], the Helium Plasma Ionization source (HePI)[5], the Flowing Atmospheric-Pressure Afterglow (FAPA)[6], the Plasma-Assisted Desorption/Ionization (PADI)[7], and the dielectric barrier discharge (DBD)[8] / Low-Temperature Plasma (LTP) probe.[9] They benefit most from their simplicity, flexibility, portability, absence of solvents and high chemical activity of these systems. Especially the DBD has attracted much attention in different fields of life science.[10] However, the desorption/ionization mechanism of these plasmas is not understood in detail yet. This gap between understanding and utilization is especially noticeable in the application of these plasmas as ionization sources for mass spectrometry. Without understanding how the probe characteristics affect the ionization performance, the entire range of compounds, the DBD may be suitable for, cannot be completely discovered and improved.

The DBD set-up originally employs a capacitively coupled discharge between a pin and a plate with the sample positioned on a dielectric substrate placed between the electrodes.[8] This direct exposure of solid or liquid sample to the nascent plasma, however, leads to a high degree of fragmentation.[8] Therefore, further development yielded in indirect sample introduction approaches, where the plasma merely excites a gas stream which is then used for desorption/ionization. The discharge region is dominated by a large number of microdischarges and therefore, the breakdown is strongly heterogenous, resulting in a rather low ambient gas temperature up to < 300 K.[10] Chemically reactive species such as high-energy electrons, metastable neutrals and radical ions/neutrals are generated, which subsequently transfer charge onto the analyte. Except for significantly lowering the yields of unwanted fragmentation products, the indirect operation further benefits from minor matrix effects and allows for ambient MS applications.[9] Nevertheless, the DBD probe experiences a typical drawback known from other ambient ionization sources. The ionization source is typically placed in the immediate vicinity of the inlet nozzle to compensate for ion loss due to atmospheric collisions. These geometrical restrictions result in a rather complicated sample handling. Since most plasma probes are operated with helium as discharge gas, this leads to higher technical demands regarding the vacuum system which is disadvantageous in context of portable mass spectrometers.

In the indirect sample introduction scheme the plasma has to provide the energy for both: sample desorption and charge transfer for an effective analyte ion formation. Mechanistic studies of plasma-based ionization sources can be therefore divided into two main subjects: desorption process and ionization process. For comprehensive and detailed summary recent reviews by Guo *et al*. and Albert *et al*. are recommended.[1,11]

As in other ambient techniques, the mere sample pick up is favored even by mildly elevated carrier gas temperatures[9], thus, throughout the literature a thermal desorption is discussed to be the predominant mechanism. *Nota bene* the thermal influence refers to the kinetic rotational and vibrational temperatures, in which nuclei are displaced since they carry the main momentum. In strong contrast are the electronic temperatures that can be evaluated *via* a Boltzmann analysis of the optical emission spectra. Despite the mild conditions and the low overall heat, electronic state populations in DBD can easily correspond to electronic temperatures of several thousand Kelvin. Opposing the sample desorption this electronic excitation is commonly accepted to be the driving force for ion formation and has already been used as an analytical device for elemental determination *via* optical emission spectroscopy.[12]

Optical spectroscopy experiments[12,13] showed the state distributions inside the plasma and, thus, also the ionization efficiency in MS-experiments to strongly depend on external parameters of the plasma source. Over the years the main influences could be identified to be briefly: (1) the torch geometry, including the material and arrangement of the electrodes and the dielectric[9,14–17], (2) type and flow rate of the discharge gas[8,13], as well as the use of additives[18,19] and (3) the high voltage pulse characteristics.[20] Based on a comprehensive study on the influence of the applied voltage, Franzke and co-workers postulated two individual operational modes in which current flows: a homogenous

and a filamentary moiety[21] that can be selectively discriminated against by altering the driving voltage.[22,23] These modes were classified to go along with a soft ionization with hardly any fragmentation for the homogenous mode (at low voltages) and a more harsh ionization that leads to considerable dissociation for the filamentary operation (driven by higher voltages), respectively. Shelley *et al*. demonstrated the waveform shape also having an influence on the plasma mode. Filamentary discharges that appear to be capacitively driven occur at times when the temporal derivative of the voltage is large, while homogenous discharges are driven by a steep change in the voltage directly. They also observed a dependence of the type of preferential discharge behavior on the formation of charge transfer with respect to proton transfer products.[20] These findings may make accessible an ionization source that can - without the necessity of undertaking geometrical changes - be operated in both modes, depending on the polarity and the chemical inertness of the analyte of interest.

In the present study, this goal is being introduced using a small, but effective DBD gas source consisting merely of disposable low-cost products. Both operational modes are spectroscopically and spectrometrically characterized and their applicability is tested on exemplary analytes. Based on the above mentioned, a switching between the individual modes can be utilized by either changing the applied voltage or the gas discharge flux. Both modes are shown to yield in an efficient ion formation. While the homogenous operation results in the well-known protonated species, ammonium adducts (most likely from the ubiquitous atmospheric N_2) can be identified as the primary product channel in filamentary operation. Surprisingly, none of the operational modes resulted in any significant fragmentation of the analyte molecules.

Experimental

Safety

Special care is required throughout when working with high voltage power supplies. The risk of an electric shock is substantial. Appropriate electrical shielding of the high voltage lines must be considered.

Chemical reagents

Ultra-high purity helium (99.999%, Linde, Duesseldorf, Germany) and nitrogen (99.99%, Air Liquide, Berlin, Germany) were used as discharge gas throughout the experiments. Aqueous ammonia solution (20/22%, Fisher Scientific UK, Loughborough, Great Britain), acetone (synthesis grade, AppliChem, Darmstadt, Germany) and ferrocene (98%, Acros Organics, Geel, Belgium) were used directly without further purification.

Dielectric barrier discharge probe

The home-built dielectric barrier discharge probe used in these studies consists of a simple toolbox, resulting in the possibility of a rapid change of different working modes. The individual parts are all commercially available mass products and entirely disposable. In consequence, an efficient, low-cost (<250€), continuous ionization source in combination with an atmospheric pressure interface time-of-flight mass spectrometer was developed (*cf.* Fig. 1)

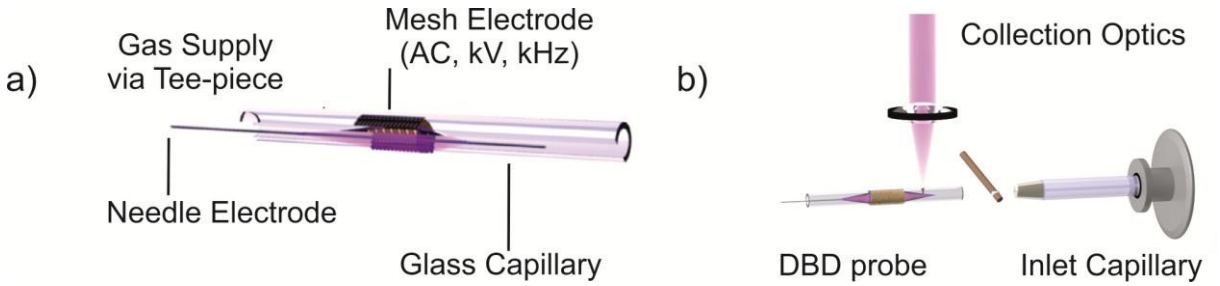

Fig. 1 (a) DBD probe and (b) Schematic of the used setup. The DBD probe was positioned coaxial to the inlet capillary of the mass spectrometer. Installed above the plasma probe, collection optics and an optical fiber connected to a Czerny-Turner spectrograph were placed for optical characterization of the plasma via emission spectroscopy.

Copper mesh (1 mm x 1 mm) of 1 cm width was placed outside of a borosilicate quartz capillary (GB 150-8P, 1.50 mm o.d.,0.86 mm i.d., Science Products GmbH, Hofheim, Germany) and serves as the high-voltage electrode. An acupuncture needle made of stainless steel (NSP 3070 Premium Silver Handle, length: 10 cm Akupunkturnadeln-Wandrey GmbH, Berlin, Germany), which served as the grounded counter electrode, was placed inside the quartz capillary. A 1/16" Swagelok Tee-piece and Teflon sealing band was used to fix the position of the grounded electrode and the inlet of the discharge gas. The discharge gas streams through the glass tube to facilitate the discharge and to support the transmission of analyte ions towards the inlet capillary. Gas flow was monitored and adjustable from 0 L min^{-1} to 2.0 L min^{-1} using a mass flow meter (GFC17, Analyt-MTC GmbH, Müllheim, Germany). Unless stated otherwise a flow rate of 1.0 L min^{-1} was used. No additional heating of the discharge gas stream was applied. High voltage is provided by a low-cost flyback high voltage transformer (PLASMSP_v2, Voltagezone Electronics e.U., Graz, Austria) fed by a standard laboratory power supply (Voltcraft PS 2403 Pro, Conrad Electronic, Germany). This specific generator setup was capable of producing an up to 15 kV_{pp} sine waveform at a frequency of 120 kHz. The applied voltage was monitored with a high-voltage probe (Voltcraft H 40, Conrad Electronic, Germany) connected to a digital oscilloscope (TDS 2024B, Tektronix, Beaverton, OR, USA). Current waveforms were recorded by measuring the voltage drop across a 1 kΩ resistor connected between the powered electrode and the ground.

Mass spectrometry

All experiments were conducted using a modified atmospheric pressure interface, orthogonal time-of-flight mass spectrometer (API-HTOF, Tofwerk, Thun, Switzerland). The instrument comprises three differential pumping stages equipped with RF and DC ion guiding and focusing optics, which were sequentially passed. Transfer into the first pumping stage (~10^{-1} mbar) of the mass spectrometer is achieved directly with an atmospheric pressure inlet capillary (6.5 mm o.d., 0.6 mm i.d., length: 150 mm, Photonis, Sturbridge, Massachusetts, USA), held at room temperature. Independent voltages could be applied to the entrance capillary. However, best signal stability was achieved when the electrode was grounded. Ion guidance into the second pumping stage (~10^{-5} mbar) is achieved through a skimmer/einzel lens combination. To minimize the ion loss due to the occurring spray cone, the outlet of the inlet capillary was fixed in direct vicinity of the skimmer. The third pumping stage (~10^{-7} mbar) is equipped with a skimmer/notch filter combination to support the ion transport into the drift zone. Throughout all experiments the notch filter was not in use. To ensure that the vacuum system could cope with the higher helium flux, the primary set-up has been equipped by a second dry scroll vacuum pump in the first pumping stage (Varian TriScroll 600, Varian Inc. Vacuum Technologies, Lexington, MA, USA) and an additional turbomolecular drag pump (Pfeiffer TMH-065, Pfeiffer Vacuum GmbH, Germany) in the second pumping stage. The instrument was operated in single reflectron geometry using the positive ion mode.

The DBD probe was axially placed in front of the inlet capillary on a multidimensional stage which allows for an easy geometric alignment. The free space distance between both capillary ends was set

to 2 cm, which is relatively large compared to other ambient ionization sources and facilitates sample handling and additional instrumentation. Note further that the DBD capillary end itself protrudes 3 cm from the discharge. This setup ensures only the excited gas stream interacts with the sample and promotes the desorption/ionization process and excludes a direct sample/plasma interaction.

Sample Analysis

Pure analyte samples were deposited on the wooden handle of cotton swabs and were exposed directly at the midpoint between DBD probe and the inlet capillary of the mass spectrometer. Averaged spectra were obtained by choosing an acquisition time of 10 s and an extraction rate of 20 kHz using the TofDaq Software package.

Emission Spectroscopy

For the spectral analysis of the plasma discharge, a Czerny-Turner spectrograph (Shamrock sr-303i, ANDOR Technology Ltd., Belfast, UK, 600 lines grating), equipped with a CCD camera (iDus CCD camera, Andor Technology Ltd., Belfast, UK, - 60°C) was used. Slit width was 150 µm and acquisition time was set to 2 s. Emitted light was collected from the top of the discharge region via a fiber placed at a distance of 20 mm from the powered electrode. For a better visualization of the emitted light, a spatially resolved spectral mapping experiment was also conducted. The emitted light was imaged onto the entrance slit (width: 50 µm) of the spectrometer and the 2D images were obtained slice-by-slice using step size of 250 µm. Acquisition time was increased to 4 s.

Results and Discussion

The low-cost flyback transformer in combination with an adjustable laboratory power supply enables the performance of the source to be examined with varying voltages. Throughout this paper, the discharge was operated at two different working modes: a homogeneous glow discharge at 5 kV_{pp} and a filamentary glow discharge at 15 kV_{pp}. The chosen power supply generates a sine waveform with a frequency of 120 kHz. In most earlier studies DBD based ion sources were limited to a maximum voltage of about 6 kV_{pp} and lower frequencies.

Blank spectrum analysis

An example of the reagent-ion spectrum of the homogeneous mode is shown in Fig.2 a). The ion pattern resembles those previously detected for other ambient plasma-based ion sources, such as He-induced DART[24] and the microplasma ionization source.[25] Most abundant background ions stem from a series of protonated water clusters $[(H_2O)_nH]^+$, with n = 2, 3 and 4. The production of protonated water clusters in helium-driven plasmas is well-known. In presence of a molecule with higher proton affinity, these protonated water clusters undergo efficient proton transfer reactions yielding the protonated molecular ion $[M+H]^+$. It is known that proton affinities of $[(H_2O)_nH]^+$ increase with n.[26] Further it could be shown that clusters with n = 2 and 3 present larger reaction cross sections for the proton transfer relative to water clusters of higher masses under vacuum conditions. [27] Therefore abundance of cluster ions with n = 2, 3 should be advantageous for an efficient proton transfer.

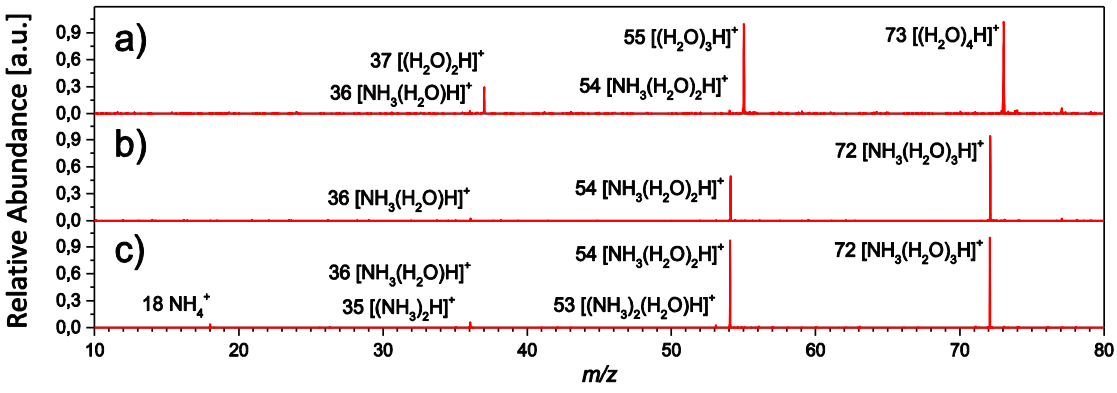

Fig. 2: MS background spectra using (a) the homogeneous mode at 5 kV_{pp} and (b) the filamentary mode at 15 kV_{pp} of the DBD probe operated with He. The main features within the homogeneous mode are protonated water clusters. In contrast, the filamentary mode resembles a series of ammonia water clusters. Spectrum (c) depicts the steady-state signal from the N_2 plasma in filamentary mode being also dominated by ammonia water clusters.

Typical formation for charge-transfer promoting ions, such as NO^+ and O_2^+ was not detected throughout the use of the setup shown here. Therefore the DBD probe was also tested with another inlet system presented earlier in (*cf.* Fig. S1).[20] The obtained spectrum exhibits compared vast similarity to FAPA[28] and LTP[20] spectra. Also here, most abundant background ions stem from protonated water clusters. Additionally signals at *m/z* 30 and 32 indicate the formation of NO^+ and O_2^+, which could potentially promote charge transfer interactions to form ions from non-polar molecules. Other ionic species in lower abundance were identified to be *m/z* 46 NO_2^+, *m/z* 48 O_3^+, *m/z* 33 O_2H^+ and *m/z* 29 N_2H^+.[29]

The reagent ion spectrum in filamentary mode is shown in Fig. 2 b). Albeit not visible in the normalized representation in the figure, a striking change is the increase in the detected total ion current of factor 3. This stark increase in overall ionization yield goes along with an increased number of formed ion species over which the induced charge distributes. Hence, compared to figure 2 a) the single species ion signal (e.g. m/z 72 in fig. 2 b) compared to m/z 73 in figure 2 a)) experiences an increase in signal intensity of factor 10. This finding suggests a significant increase in sensitivity by applying a higher driving potential. Please note, that this 10-fold signal increase goes along with a merely 5-fold rise in electrical power consumption (~ 1 W for recording fig. 2 a); ~ 5.5 W for recording figure 2 b)) of the discharge setup. This ratio between ion yield and power consumption most likely stems from a larger duty cycle of the higher voltage plasma mode which may result in smaller dissipation into competitive ion loss channels compared to the short lived plasma bullets in homogeneous discharge mode.

In contrast to the spectrum depicted in Figure 2 a), the spectrum obtained at higher voltages is dominated by even numbered clusters, *e.g. m/z* 36, 54, 72 and 90, whereas signals for protonated water clusters usually have quite low abundance or are completely absent. In helium-driven plasmas species such as He_m, He_2^+ and high-energy electrons are present.[12] Each of these species carries enough internal energy to sufficiently ionize H_2O (IE = 12.6 eV) to be $H_2O^{\cdot+}$. Thus, it could be incorporated in the formation of even-numbered clusters. However, in presence of water $H_2O^{\cdot+}$ will convert quickly to H_3O+ due to autoprotonation.[36] Therefore, the ions of 36, 54, 72 and 90 are more likely to be clusters in the form of $[NH_3(H_2O)_nH]^+$ than radical water clusters $[H_2O]_n^{\cdot+}$. The ammonium ions may originate from either trace amounts of ammonia in the laboratory environment or are more likely formed via plasma interaction with ambient N_2 and H_2O. Ammonia formation has been previously described by Fujii *et al.* using a gas mixture of N_2/H_2 in a microwave plasma.[30] They claimed that N_2H^+ plays an important role as a precursor ion, which can be also spectrometrically identified in Fig. S1 using the dual mode DBD. Further experiments were carried out for an unambiguous identification: (1) high-resolution TOFMS, (2) addition of an aqueous ammonia solution into the region between probe and inlet capillary and (3) using N_2 as discharge gas.

Via high-resolution mass spectrometry mass differences of even numbered and odd numbered clusters in different mass regions were calculated and compared to theoretical calculated mass differences for the speculated reagent-ions (*cf.* Fig. S2). As a result, NH_4^+ was identified. Additionally, NH_4^+ formation was monitored using the change of the specific ion current chronograms upon addition of ammonia into the interaction region of the plasma (*cf.* Fig. S3). A new series of signals was immediately observed and assigned to $[(NH_3)_nH]^+$ (*cf.* S2). Additionally, stable plasma in filamentary mode was ignited using pure N_2. The obtained mass spectrum reveals comparable results to that shown for the helium-driven plasma probe in filamentary mode (*cf.* Fig. 2).

To obtain a comparable performance, optimal experimental parameters were chosen as follows: flow rate had to be increased to 2.0 L min^{-1}. Further, the distance between the inlet capillary and the probe was decreased to 1.0 cm. Additionally, the steady-state signal reveals a new series of clusters based

on protonated ammonia clusters: *m/z* 35 $[(NH_3)_2H]^+$ and *m/z* 53 $[(NH_3)_2(H_2O)H]^+$. Note that no signal for protonated water clusters could be obtained by varying experimental parameters, such as the gap distance, electrode geometry, flow rate, as well as the pressure gradient in the first differential pumping stage of the mass spectrometer.

Interestingly, the results obtained in the higher-voltage mode are most consistent with data observed with microwave induced plasma mass spectrometry (MIPI)[31], although MIPI requires rather harsh conditions in terms of power consumption and used frequency. NH_4^+ formation could especially be influenced using the additional N_2 sheet gas flow of their mass spectrometer. Further, pronounced formation of NH_4^+ clusters has been shown for DART using both, helium and nitrogen as discharge gas, confirming the current observations.[32] It has been observed that in helium-DART NH_4^+ formation became more favorable at lower gas temperatures. Using nitrogen as discharge gas only NH_4^+ adducts were detected.

Going into more detail, evidence for the formation of NH_4^+ to certain different extents can be found in many other ambient plasma-based ionization sources, *e.g.* LTP[11], FAPA[24], microplasma discharge ionization[25] and PADI[33]. Even though all these ionization techniques named here are somehow different in terms of their experimental parameters they seem to share some common features. In very few cases NH_4^+ is considered to be another source for protons with a higher proton affinity than NH_3 but can also form adduct ions $[M+NH_4]^+$.

Current/Voltage Profiles

In a recent study Shelley *et al.* demonstrated that different waveforms heavily influence the discharge properties and consequently the ion production in LTPs.[20] Fig. 3 depicts three selected current waveforms of the switchable plasma probe fed with different voltages and discharge gases. Waveform (a) and (b) were recorded using He as the discharge gas and represent the two moieties discussed throughout this study: the homogeneous mode and the filamentary mode, respectively. For further insights into the ongoing mechanism, the filamentary mode using N_2 as discharge gas is shown in (c).

The spectrometric experiments already revealed the two individual discharge regimes to be capable of producing different reagent ions: protonated water clusters in homogeneous mode and ammonium water clusters in filamentary mode. As can be seen from Fig. 3, both modes produced stable discharges with very reproducible events. However each regime showed a distinctly different discharge pattern of current waveforms which were highly dependent on the provided total voltage. Further, the individual waveforms indicate that each half cycle produced short-lived discharges at each transition between the positive and negative voltage. In case of the homogeneous mode (1 W, 5 kV_{pp}) only isolated, regularly distributed discharge events occur at times of change of sign of the voltage. Similar behavior has been observed for squarewave or sawtooth driven plasmas.[20] These consistent current pulses may indicate the formation of plasma bullets, which are high-velocity ionization waves known to occur with DBDs.[20] The discharge occurring at the zero crossing of the applied voltage indicates the nature of the discharge to be inductively driven. As the applied voltage increases, a greater number of erratic current pulses were observed. The detailed process of switching between both moieties can be followed in Fig. S4. In filamentary mode (5.5 W, 15 kV_{pp}) current spikes were more frequent due to the increasing voltage change. The current waveform is dominated by a variety of many short sporadic plasma pulses, accompanied by a minor number of prominent stronger discharges. However, even the smaller microdischarges carry higher current compared to 3(a). They appear with a large duty cycle, hence resulting in the production of a higher number of reagent ions. A closer inspection of the temporal behavior of the discharge occurrence reveals the breakdown to happen at times of potential maxima/minima. These are the times at which the potential different between the two electrodes reach their maximum. Therefore, this current is most likely capacitively driven. In the remainder of this article the two plasma modes will therefore be considered inductively (homogenous plasma) and capacitively (erratic filamentary plasma) driven, respectively.

Based on these observations, the discharge behavior reflects the switchable ion formation of protonated species and ammonium species. Additionally the current waveform of a N_2 plasma in filamentary mode can be adduced to support the experimental results for the He discharge. The signal pattern strongly resembles the current waveform found in Fig. 3(b).

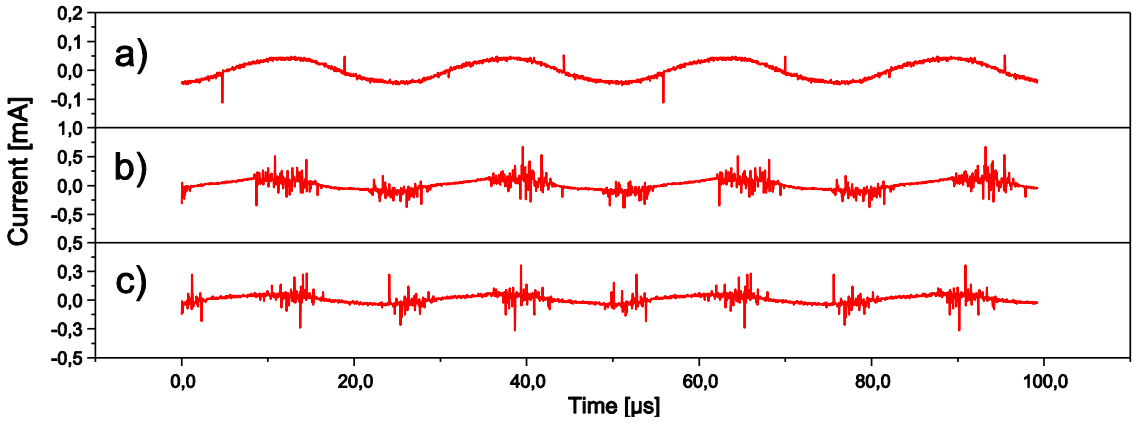

Fig. 3: Current waveforms at different voltages: (a) homogeneous mode at 5 kV_{pp} and (b) filamentary mode at 15 kV_{pp} operated with He as discharge gas. For comparison the resulting current waveform of a filamentary mode using N_2 is depicted in (c).

Spectroscopic characteristics and identification of plasma species in He-DBD

Optical characterization of the discharge can yield further insight into the plasma/gas reactions. The identification of reactant species present in the plasma helps to shortlist the possible candidates that are likely involved in the different ionization pathways. Therefore a better understanding of the mechanism by which the DBD operates can be achieved, but also optimization of DBD performance as ionization source for mass spectrometry can be envisioned.

Fig. 4 shows the UV-visible emission spectra of the discharge region in either inductive or capacitive mode, integrated along the vertical axis of the He DBD probe under above mentioned conditions. In the lower wavelength region strong molecular emission from several vibronic progressions of N_2^+ (B $^2\Sigma_u^+ \rightarrow$ X $^2\Sigma_g^+$) were present in both modes. However, contributions that stem from excited neutral N_2 (C $^3\Pi_u \rightarrow$ B $^3\Pi_g$) and the (0,0) band head of OH (A $^2\Sigma^+ \rightarrow$ X $^2\Pi_i$) can be observed only in filamentary mode. Furthermore, emission lines of the atomic species: H_α, H_β, and He I can be readily attributed. These species nicely resemble the composition of other types of He discharges operated at atmospheric pressure.[6,12,13,17,34–37] The presence of non-helium species was attributed to impurities in the gas supply, as well as diffusion from the ambient into the borosilicate capillary. Molecular emission from N_2^+ is observed to be more intense than the spectral N_2 contribution, which is in agreement with previous findings, claiming that N_2^+ is a key intermediate for ion formation. In contrast to other ambient plasma sources, no emission from other reactive oxygen and nitrogen species, like NO[6] and CN[38] could be observed. Likewise observation of emission from NH was not observed. Even though it could be another indicator for the formation of ammonia in the plasma, the life time of the NH radical is too short. The near IR line of O I in the capacitive mode (not shown in the spectrum) was found to be much weaker than in other He driven plasma sources.[17] The absence of oxidating species could account for a mild ionization with only minor fragmentation when used as an MS ionization source.[24]

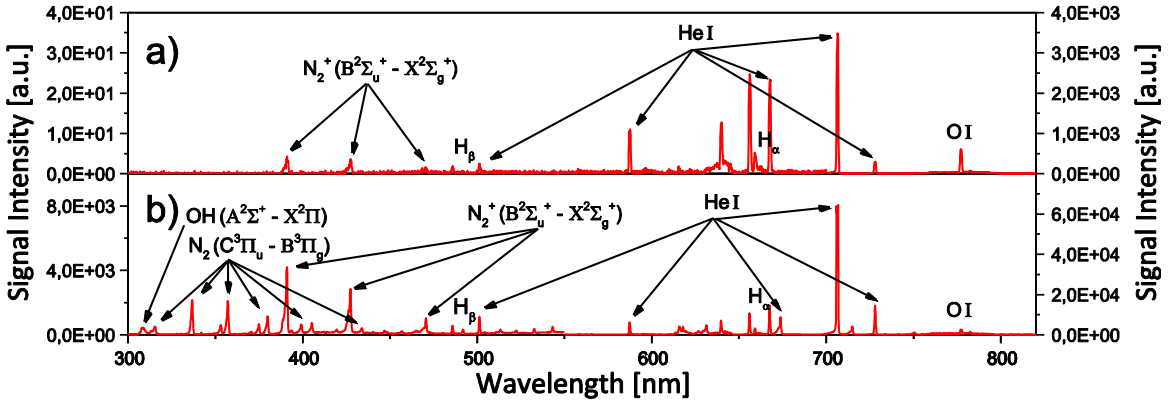

Fig. 4: UV/Vis spectra obtained from the He driven plasma probe in (a) homogeneous and (b) filamentary mode. Atomic lines and molecular bands of interest have been labeled. Please note the unassigned peaks between λ = 600 nm and 750 nm are first order artefacts of the N_2 ($C\ ^3\Pi_u \rightarrow B\ ^3\Pi_g$) progression which is detected in the second blazing order of the spectrograph. Due to different transition probabilities of the individual progressions the intensity scale has been split. For the upper spectrum, the scale on the left hand side represents the intensity of the spectral part between λ = 300 nm and λ = 700 nm, the intensity above λ = 700 nm is given on the right hand side axis. The scale on the left hand side in spectrum b) represents the intensity of the spectral part between λ = 300 nm and λ = 550 nm, the intensity above λ = 550 nm is given on the right hand side axis.

Spectroscopic characteristics and identification of plasma species in N_2-DBD

As discussed above, the use of nitrogen as discharge gas revealed similar characteristics as the filamentary mode of the He DBD. Therefore the plasma jet was operated with N_2 and the reactive species were observed by their characteristic emission lines (*cf.* Fig. 5). Rather surprisingly, the N_2 DBD exhibits an entirely different spectral pattern. The only shared feature is the emission of the excited neutral N_2 molecule ($C\ ^3\Pi_u \rightarrow B\ ^3\Pi_g$). No emission of N_2^+, OH, H and O was observed.

The $C\ ^3\Pi_u$ state of N_2 can either be populated directly from the $X\ ^1\Sigma_g$ ground state via electron impact excitation or by electron capture relaxation of the $N_2^+\ X\ ^2\Sigma_g^+$ ionic state. However, in accordance with earlier results of a nitrogen driven discharge by Qayyum *et al.*[39], no $N_2^+\ X\ ^2\Sigma_g^+$ could be observed. Thus, the direct excitation of ground state molecular nitrogen is the only remaining pathway, while the N_2^+ formation in He plasma is likely to be formed by Penning ionization between He metastables and neutral N_2.

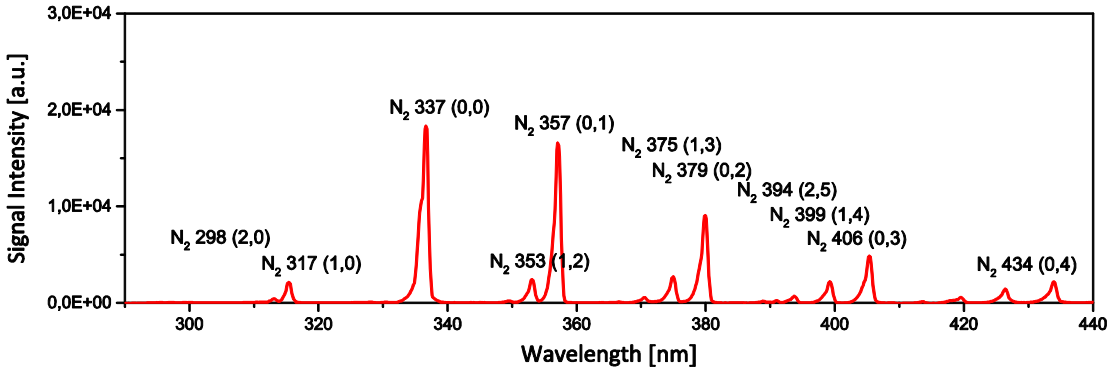

Fig. 5: UV/Vis spectrum obtained from the N_2 discharge using a flow rate of 2.0 L min^{-1}. The spectrum is dominated by strong molecular emission from excited neutral N_2 ($C\ ^3\Pi_u \rightarrow B\ ^3\Pi_g$). Emission from additional reactant species was not observed.

The presented results clearly show a distinct difference in the formation of reactive species in the two different discharge gases. While in the N_2 discharge only the electron temperature determines the upper limit of populated species, the energetically high lying electronic and Rydberg states of He open a plethora of additionally energetically accessible states of involved species. This finding is at first somewhat counterintuitive, since the involvement of more reactive species – many of them with a huge oxidative potential – should result in greatly favoured fragmentation. However, throughout the literature He discharges are discussed to form the chemically "cleaner" spectra.

Also, from the observed emission spectra one mechanistic limitation can directly be derived. The production of water clusters is directly coupled to the density of the inital reactive nitrogen that begins the known APCI cascade. The complete absence of N_2^+ emission in the N_2-DBD excludes this well established reaction pathway as a source of protonated water clusters. Consequently we suggest that excited neutral nitrogen can act as an additional ambient molecular ionization agent in DBDs.

Controlled formation of reactive species

Results from N_2-DBD characterization show that neutral excited molecular N_2 opens an additional pathway in plasma chemistry for the formation of ammonium water clusters. Since emission from the second positive system of N_2 is also present in He DBDs, it is favorable to investigate if the He driven DBD could create both species discussed above specifically for purpose. Significant parameters that affected primarily the reagent ion formation in He DBD included the applied voltage and the plasma gas flow.

Voltage-dependent ion formation

Two different reactant species have been observed within the dual mode He DBD: protonated water clusters which are well-known to be produced in plasma-based ionization sources and ammonium-based clusters. However, the explicit formation of ammonium ions has been described in only few publications. Further, the possibility of a direct formation of ammonium in a dielectric barrier discharge has not been considered yet as an additional reaction channel. Fig. 6 depicts the voltage-dependent signal intensities for $[NH_3(H_2O)_4H]^+$ (*m/z* 90) and $[(H_2O)_4H]^+$ (*m/z* 73), respectively. The left part of the graph, covering the lower voltage region (4 kV_{pp} - 7 kV_{pp}) reflects the most common mass spectra appearance for most other plasma-based ionization sources. Most abundant background signal stems from protonated water clusters which undergo efficient proton transfer reactions yielding the protonated molecular ion $[M+H]^+$, while ammonium species have usually lower abundance or are completely absent. Further increase of the applied voltage to the plasma eventually leads to an inversion of the concentrations of the reactive species, resulting in excess of ammonium clusters. Thus, using this operational mode the analyte is typically observed as an ammonium adduct.

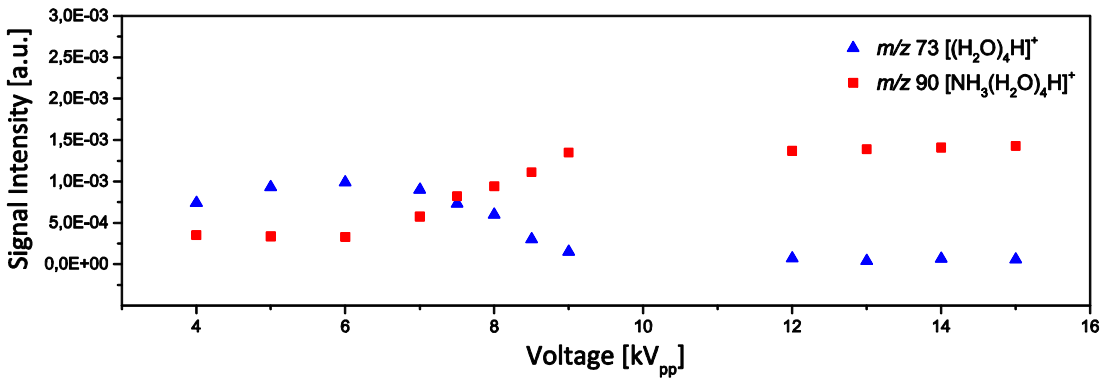

Fig. 6: Voltage-dependent signals for the ammoniated water tetramer $[NH_3(H_2O)_4H]^+$ at *m/z* 90 and the protonated water tetramer $[(H_2O)_4H]^+$ at *m/z* 73. At lower voltages the DBD is operated in homogeneous mode forming primarily protonated water clusters. With an increase in voltage the a second reaction pathway towards the formation of ammonium clusters is favored.

Flow-dependent ion formation

Previous studies on the influence of the plasma gas flow on emission features of the LTP probe has been presented by Chan *et al.*[17] in which the He flow rate was varied from 0.40 L min^{-1} to 1.60 L min^{-1}. Their findings imply that a greater concentration of high-energy helium species, which are ultimately responsible for the formation of key reactant species (*e.g.* N_2^+), can be produced outside of the torch, simply by increasing the He flow rate.

Therefore, the plasma gas flow of the previous set-up has been also examined with respect to the different discussed reaction channels: formation of either ammonium water clusters in filamentary mode or protonated water clusters in homogeneous mode (*cf.* Fig. 7). The ratios given here were calculated by using the signal intensity of the protonated water tetramer $[(H_2O)_4H]^+$) (*m/z* 73) and its corresponding ammonium water cluster $[NH_3(H_2O)_4H]^+$ (*m/z* 90), respectively. For each spectrum the acquisition time was increased to 60 s. In the capacitive mode the gap between DBD and MS was held at 2.0 cm, while in inductive mode the distance had to be reduced to 1.0 cm due to an overall lower ion count using lower voltages (not shown here). Throughout the experiment the helium flow rate was adjusted in 0.05 L min^{-1} steps using a gas flow meter. Results for the homogeneous mode are depicted as blue triangles and red dots for the filamentary mode.

Regarding the observed ratios, both operational modes showed similar trends. The formation of ammonium water clusters clearly benefits from lower flow rates and thus, longer dwell times. In contrast, the pathway for protonation is favored with an increase in the flow rate and a lower dwell time. This result goes along with a more effective energy transfer into the present gas, eventually sufficing for a breaking of the N_2 triple bond. This fragmentation/atomization is most likely to occur in the outmost upstream region of the gas stream, for spatially resolved spectroscopy mapping revealed the largest electronic temperatures here (*cf.* Fig. S5) Note that for both options even at higher flow rates signal for ammonium water clusters were still present, but to a significantly lower extent. However, similar trends were observed. The voltage difference affects the individual graphs for each mode to be shifted along the *x*-axis. In consequence, formation of ammonium water clusters in the homogeneous mode started to become more dominant below 0.5 L min^{-1}, while in filamentary mode the same trend already started at about 1.2 L min^{-1}. Further, both modes were restricted to a minimal flow rate to avoid a capillary meltdown and direct arc formation. Stable plasmas could be ignited in homogeneous mode starting from 0.2 L min^{-1} and 0.6 L min^{-1} in filamentary mode. Thus, experimental parameters could be chosen to define a known chemical environment in which the analyte is ultimately ionized.

Earlier observations made by Chan *et al.* resemble the recent findings.[17] The strong formation of ammonium ions suggests that an active migration of atmospheric components (*e.g.* N_2, O_2, H_2O) into the dielectric capillary is present. Smaller contribution could further stem from impurities in the used discharge gas. We suggest that with a decreasing helium flux, migration towards the discharge region is facilitated and therefore a higher amount of ammonium ions can be directly formed in the plasma.

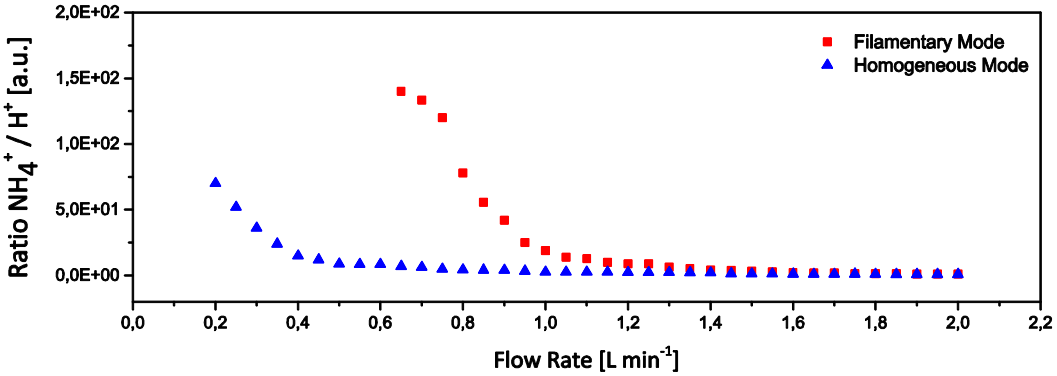

Fig. 7: Calculated signal intensity ratio of $[NH_3(H_2O)_4H]^+$ (*m/z* 90) and $[(H_2O)_4H]^+$ (*m/z* 73) as a function of He flow in both: homogeneous mode and filamentary mode. At lower flow rates the formation of ammonium water clusters is facilitated, while at higher helium flux formation of protonated water clusters is favored.

Mass Spectrometry of test compounds

Performance tests in both operational modes were conducted using acetone and ferrocene as test compounds. Samples were deposited on the wooden handle of cotton swabs and were exposed directly at the midpoint between DBD probe and the inlet capillary of the mass spectrometer. Therefore only the excited gas stream interacted with the sample and promoted the desorption/ionization process. Acetone and ferrocene were used due to their large vapor pressure. At the same time ferrocene is a standard test sample for plasma-based ionization techniques since the presence/absence of fragmentation products allows a rough estimation of the plasma conditions.

As shown in Fig. 8 (a) and (b) for acetone, single ion formation $[M+H]^+$ (*m/z* 59) and $[M+NH_4]^+$ (*m/z* 76), dimerization $[2M+H]^+$ (*m/z* 117) and $[2M+NH_4]^+$ (*m/z* 134) and trimerization $[3M+H]^+$ (*m/z* 175) and $[3M+NH_4]^+$ (*m/z* 192) was observed. Additionally, with increasing *m/z* values three additional different cluster series were also present including protonated water clusters in homogeneous mode, as well as ammonium water clusters in the filamentary mode. This shift in equilibrium towards larger clusters can be rationalized by the3 higher overall proton affinity for the reagent ion system. It is commonly known that the individual proton affinities of protonated water clusters correlate directly with their size. The calculated proton affinities for $[(H_2O)_nH]^+$, with n = 2, 3 and 4 are 832, 888 and 919 kJ mol^{-1}.[26] Therefore, it is unlikely that in the homogeneous operational mode proton transfer to acetone, 812 kJ mol^{-1} [40], occurs from these species. Instead the formation of intact adducts is favored. Accordingly, in filamentary mode no single proton transfer from NH_4^+ or corresponding ammonia water clusters onto acetone can be observed, because the corresponding proton affinities for water, acetone and ammonia, raise along 691, 812 and 854 kJ mol^{-1}, respectively.[40] If compared to ammonia, acetone exhibits a lower proton affinity and therefore, adduct formation dominates the obtained mass spectra.

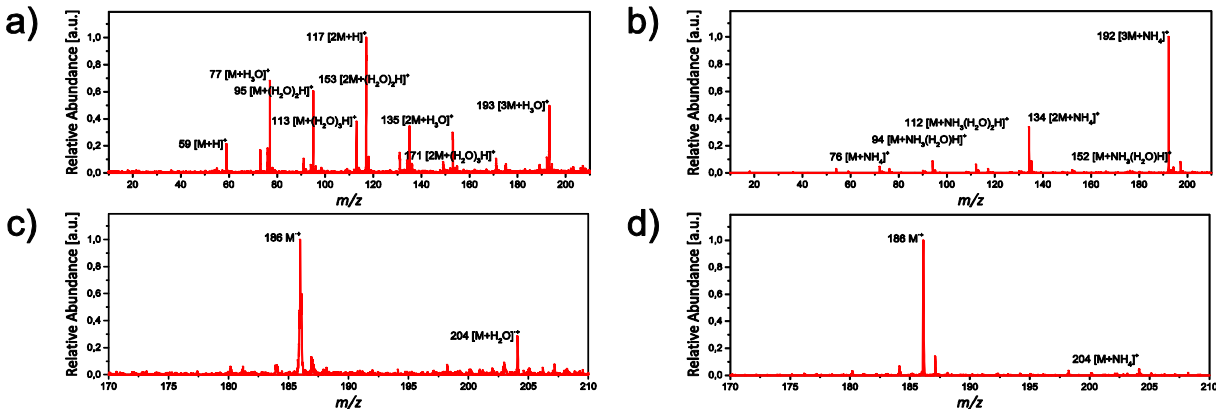

Fig. 8: MS spectra of acetone and ferrocene using homogeneous mode at 5 kV_{pp} (a), (c) and high filamentary mode at 15 kV_{pp} (b), (d).

Introduction of ferrocene into the sampling region immediately yielded in pronounced detection of the ferrocenium ion $M^{\cdot+}$ (*m/z* 186 under both plasma conditions. This can be explained due to the comparably low ionization energy of ferrocene. Additionally, adduct formation at *m/z* 204 was found. In case of the homogeneous mode, high-resolution mass spectrometry reveals that the cluster formation is most likely to be $[M+H_2O]^{\cdot+}$, while in filamentary mode the detected mass is shifted towards the NH_4^+ adduct. Overall, results obtained by mass spectrometry indicate that the signal-to-noise ratio in the homogeneous mode of the DBD probe is worse due to an overall lower total ion count. The low power discharge generates a lower abundance of reactant species, while higher voltages result in n overall larger number of discharges. Although the filamentary mode has been discussed to cause fragmentation processes, no evidence has been found here.

Conclusions

A versatile helium driven DBD has been presented, which is capable of working at two different operational modes: a homogeneous mode at 5 kV_{pp} and a predominantly filamentary mode at 15 kV_{pp}. Unlike previously known, the DBD in filamentary mode was shown to produce strong amounts of ammonium water clusters, which in consequence could form another series of important reactant ions for the ionization of analytes. Unambiguous identification of the active ammonia formation in the discharge, as well as differences between the individual operational modes were observed using means of mass spectrometry and emission spectroscopy. Whereas the filamentary mode has been already discussed in literature to induce fragmentation processes, no evidence for such pronounced effects was examined for the used test compounds. Especially the applied voltage and the helium gas flow rate showed a significant influence on the formation of either ammonium ions or protonated species. Besides the option for a specific formation of reactant ions, the dual mode DBD has potential application advantages due to its lower geometrical restrictions which enables the present system to be extended by a laser for conversion of solid material into the gas phase and a subsequent ionization via the excited gas molecules. The combination of a high-repetition rate laser and the helium driven DBD operated in filamentary mode has been already shown to succeed in a powerful tool. This combination will be the focus of an upcoming publication.

Acknowledgements

This work was financially supported by the German Federal Ministry of Education and Research (BMBF) as part of the Konjunkturpaket II. Alexander Demidov and Igor Gornushkin are gratefully acknowledged for their support regarding the optical emission experiments.

References

1 C. Guo, F. Tang, J. Chen, X. Wang, S. Zhang and X. Zhang, *Anal. Bioanal. Chem.*, 2014, **407**, 2345–2364.

2 X. Ding and Y. Duan, *Mass Spectrom. Rev.*, 2015, **34**, 449–473.

3 C. Meyer, S. Müller, E. L. Gurevich and J. Franzke, *Analyst*, 2011, **136**, 2427–2440.

4 R. B. Cody, J. A. Laramée and H. D. Durst, *Anal. Chem.*, 2005, **77**, 2297–2302.

5 Z. Yang and A. B. Attygalle, *J. Am. Soc. Mass Spectrom.*, 2011, **22**, 1395–1402.

6 F. J. Andrade, W. C. Wetzel, G. C.-Y. Chan, M. R. Webb, G. Gamez, S. J. Ray and G. M. Hieftje, *J. Anal. At. Spectrom.*, 2006, **21**, 1175.

7 L. V. Ratcliffe, F. J. M. Rutten, D. A. Barrett, T. Whitmore, D. Seymour, C. Greenwood, Y. Aranda-Gonzalvo, S. Robinson and M. McCoustra, *Anal. Chem.*, 2007, **79**, 6094–6101.

8 N. Na, M. Zhao, S. Zhang, C. Yang and X. Zhang, *J. Am. Soc. Mass Spectrom.*, 2007, **18**, 1859–1862.

9 J. D. Harper, N. A. Charipar, C. C. Mulligan, X. Zhang, R. G. Cooks and Z. Ouyang, *Anal. Chem.*, 2008, **80**, 9097–9104.

10 U. Kogelschatz, *Plasma Chem. Plasma Process.*, 2003, **23**, 1–46.

11 A. Albert, J. T. Shelley and C. Engelhard, *Anal. Bioanal. Chem.*, 2014, **406**, 6111–6127.

12 Y Yonglinag, Zh. Du, C. Mingli and W. Jianhua, *Angewandte Chemie*, 2008, **47**, 7909–7912.

13 G. C.-Y. Chan, J. T. Shelley, J. S. Wiley, C. Engelhard, A. U. Jackson, R. G. Cooks and G. M. Hieftje, *Anal. Chem.*, 2011, **83**, 3675–3686.

14 S. B. Olenici-Craciunescu, A. Michels, C. Meyer, R. Heming, S. Tombrink, W. Vautz and J. Franzke, *Spectrochim. Acta Part B At. Spectrosc.*, 2009, **64**, 1253–1258.

15 A. Albert and C. Engelhard, *Spectrochim. Acta Part B*, 2015, **105**, 109–115.

16 M. R. Almasian, C. Yang, Z. Xing, S. Zhang and X. Zhang, *Rapid Commun. Mass Spectrom.*, 2010, **24**, 742–748.

17 A. Meiners, M. Leck and B. Abel, *Rev. Sci. Instrum.*, 2010, **81**, 113507–113507–8.

18 G. C.-Y. Chan, J. T. Shelley, A. U. Jackson, J. S. Wiley, C. Engelhard, R. G. Cooks and G. M. Hieftje, *J. Anal. At. Spectrom.*, 2011, **26**, 1434–1444.

19 X. Lu and M. Laroussi, *J. Appl. Phys.*, 2005, **98**, 023301–023301–5.

20 W. S. Abdul-Majeed, J. H. L. Parada and W. B. Zimmerman, *Anal. Bioanal. Chem.*, 2011, **401**, 2713–2722.

21 J. T. Shelley, A. Stindt, J. Riedel and C. Engelhard, *J. Anal. At. Spectrom.*, 2014, **29**, 359–366.

22 H.-E. Wagner, R. Brandenburg, K. V. Kozlov, a. Sonnenfeld, P. Michel and J. F. Behnke, *Vacuum*, 2003, **71**, 417–436.

23 C. Meyer, S. Müller, B. Gilbert-Lopez and J. Franzke, *Anal. Bioanal. Chem.*, 2013, **405**, 4729–4735.

24 S. Müller, T. Krähling, D. Veza, V. Horvatic, C. Vadla and J. Franzke, *Spectrochim. Acta Part B*, 2013, **85**, 104–111.

25 J. T. Shelley, J. S. Wiley, G. C. Y. Chan, G. D. Schilling, S. J. Ray and G. M. Hieftje, *J. Am. Soc. Mass Spectrom.*, 2009, **20**, 837–844.

26 J. M. Symonds, A. S. Galhena, F. M. Fernández and T. M. Orlando, *Anal. Chem.*, 2010, **82**, 621–627.

27 Y. Kawai, S. Yamaguchi, Y. Okada, K. Takeuchi, Y. Yamauchi, S. Ozawa and H. Nakai, *Chem. Phys. Lett.*, 2003, **377**, 69–73.

28 Y. Kawai, S. Yamaguchi, Y. Okada and K. Takeuchi, *J. Mass Spectrom. Soc. Jpn.*, 2004, **52**, 271–276.

29 F. J. Andrade, J. T. Shelley, W. C. Wetzel, M. R. Webb, G. Gamez, S. J. Ray and G. M. Hieftje, *Anal. Chem.*, 2008, **80**, 2646–2653.

30 E. Marotta and C. Paradisi, *J. Am. Soc. Mass Spectrom.*, 2009, **20**, 697–707.

31 T. Fujii, K. Iwase and P. C. Selvin, *Int. J. Mass Spectrom.*, 2002, **216**, 169–175.

32 D. Li, Y.-H. Tian, Z. Zhao, W. Li and Y. Duan, *J. Mass Spectrom.*, 2015, **50**, 388–395.

33 J. J. Pérez, G. A. Harris, J. E. Chipuk, J. S. Brodbelt, M. D. Green, C. Y. Hampton and F. M. Fernández, *Analyst*, 2010, **135**, 712–719.

34 T. L. Salter, I. S. Gilmore, A. Bowfield, O. T. Olabanji and J. W. Bradley, *Anal. Chem.*, 2013, **85**, 1675–1682.

35 H. Hayen, A. Michels and J. Franzke, *Anal. Chem.*, 2009, **81**, 10239–10245.

36 J. T. Shelley, G. C.-Y. Chan and G. M. Hieftje, *J. Am. Soc. Mass Spectrom.*, 2011, **23**, 407–17.

37 Z. Machala, M. Janda, K. Hensel, I. Jedlovský, L. Leštinská, V. Foltin, V. Martišovitš and M. Morvová, *J. Mol. Spectrosc.*, 2007, **243**, 194–201.

38 Z. Zhu, G. C.-Y. Chan, S. J. Ray, X. Zhang and G. M. Hieftje, *Anal. Chem.*, 2008, **80**, 8622–8627.

39 B. Gielniak, T. Fiedler and J. A. C. Broekaert, *Spectrochim. Acta Part B*, 2011, **66**, 21–27.

40 S. Z. A. Qayyum, *J. Appl. Phys.*, 2005, **98**, 103303–103303–9.

41 E. P. L. Hunter and S. G. Lias, *J. Phys. Chem. Ref. Data*, 1998, **27**, 413–656.